Optical Fiber Strain Sensor Instrumentation for High Temperature Aerospace Structural Monitoring

NASA Award Number: NAG-1-01-018
March 2002
Final Report for Period January 01-Dec 31 02

A.Wang
Center for Photonics Technology
Bradley Department of Electrical and Computer Engineering
Virginia Polytechnic Institute and State University
Blacksburg, VA 24061-0111

CENTER FOR PHOTONICS TECHNOLOGY

TABLE OF CONTENTS

LIST OF FIGURES

Figure 2.29. Gold-coated silica fiber strain sensor is bonded on a small piece of metal part, which is welded on metal substrate.

Figure 2.30 Gold-coated silica fiber strain sensor bonded on metal substrate and two-point welding tip designed for strain sensor installation

1 Summary

The objective of the program is the development and laboratory demonstration of sensors based on silica optical fibers for measurement of high temperature strain for aerospace materials evaluations.

A complete fiber strain sensor system based on whitelight interferometry was designed and implemented. An experiment set-up was constructed to permit testing of strain measurement up to 850°C. The strain is created by bending an alumina cantilever beam to which is the fiber sensor is attached. The strain calibration is provided by the application of known beam deflections. To ensure the high temperature operation capability of the sensor, gold-coated single-mode fiber is used. Moreover, a new method of sensor surface attachment which permits accurate sensor gage length determination is also developed. Excellent results were obtained at temperatures up to 800-850°C.

2 Technical Accomplishments

2. 1 Strain Modeling

The basic concept to measure strain is to measure the displacement, ΔX between two points of a material. The distance between the two points is gauge length $X_2 - X_1$, the average strain between the two points is

$$\varepsilon = \frac{\Delta X}{X_2 - X_1} \qquad \text{----------(1)}$$

Assuming the displacement ΔX to consist of two independent potions, when temperature changes, the substrate thermal expansion will cause a displacement $\Delta X'$

$$\Delta X' = TEC_s (X_2 - X_1)\Delta T \qquad \text{----------(2)}$$

where, TEC_s is the thermal expansion coefficient of the substrate. At the same time, external load-induced mechanical stresses can also produce a

displacement $\Delta X''$ between the two points. Assuming the two displacements are independent parameters. The total displacement can be expressed as

$$\Delta X = \Delta X' + \Delta X'' \qquad \text{---------- (3)}$$

For an actual high temperature strain measurement, through the measurement of the total displacement ΔX, the strain can be calculated. If the average coefficients of the thermal expansion (CTE) of the material and the silica fiber used for the sensor are known, the total strain can further be separated into thermal and mechanical strains.

2. 2 Sensor principle

The basic principle of the white light fiber optic interferometer is illustrated in Figure 2.1. The light from a broadband light source, such as a light emitting diode (LED), is transmitted to the sensor probe, which is made by inserting two fibers with cleaved end faces into a capillary glass tubing. The two fiber ends separated by an air gap form a typical Fabry-Perot interferometric cavity. The partially reflected optical waves at these two end faces generate interference signals, detected by a fiber spectrometer.

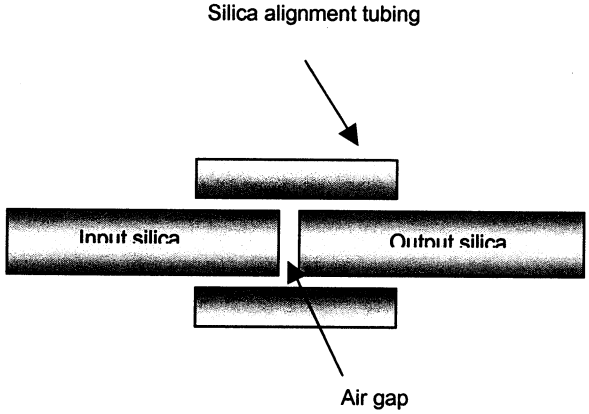

Figure 2.1. Cross section of silica fiber head

The output interference signal in the spectral domain can be expressed as

$$I = 2I_s(\lambda)\left[1+\gamma(L)\cos\left(\frac{4\pi L}{\lambda}+\varphi_0\right)\right] \qquad \text{----------(4)}$$

Where $I_s(\lambda)$ is the source spectrum, γ is the visibility coefficient, which takes into account the decreased visibility due to the numerical aperture of the fiber as well as other attenuating effects. L is the cavity length, and φ_0 is the initial phase difference between the two interference signals. Figure 2.2

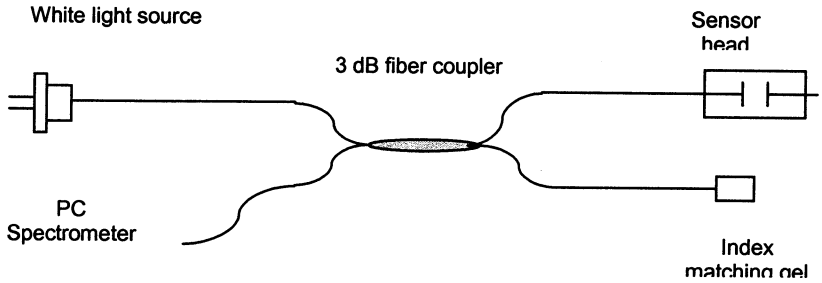

Figure 2.2. Schematic of the sensor system.

It is shown in Equation (4), that the spectrum output by the sensor is modulated by a sinusoidal function due to the inference. Figure 2.3 shows the interference spectrum (a), and the interference spectrum normalized by the original source spectrum (b), respectively. Because the interference spectrum is a function of the sensor air gap length L, the successful demodulation of this spectral signal can render an accurate and absolute measurement of the sensor air gap length.

A simple case can be considered, in which two different spectral components of the source (λ_1 and λ_2) are utilized. These two wavelength components arrive at the spectrometer with different phases, which can be express as

$$\varphi_{1,2} = \frac{4\pi L}{\lambda_{1,2}} + \varphi_0 \qquad \text{----------(5)}$$

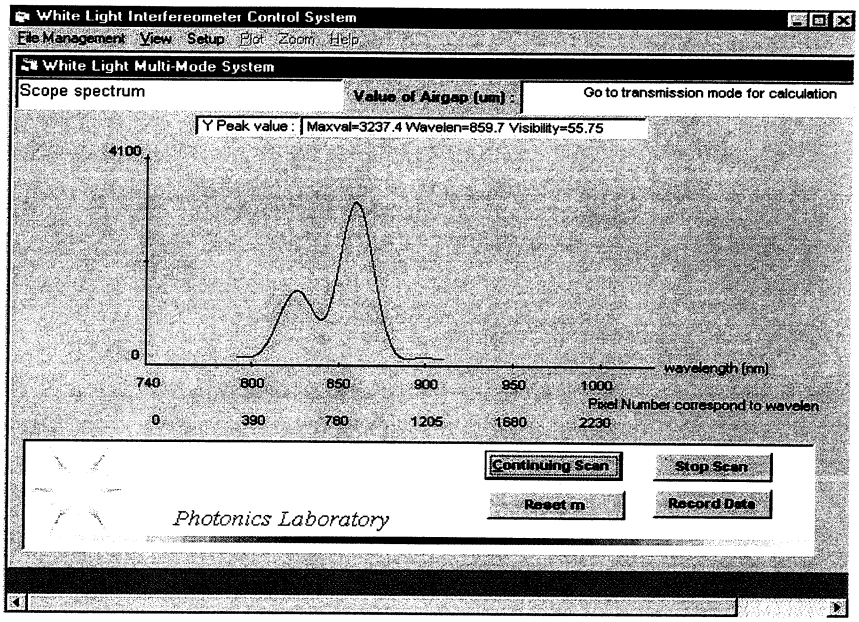

(a) Interference spectrum

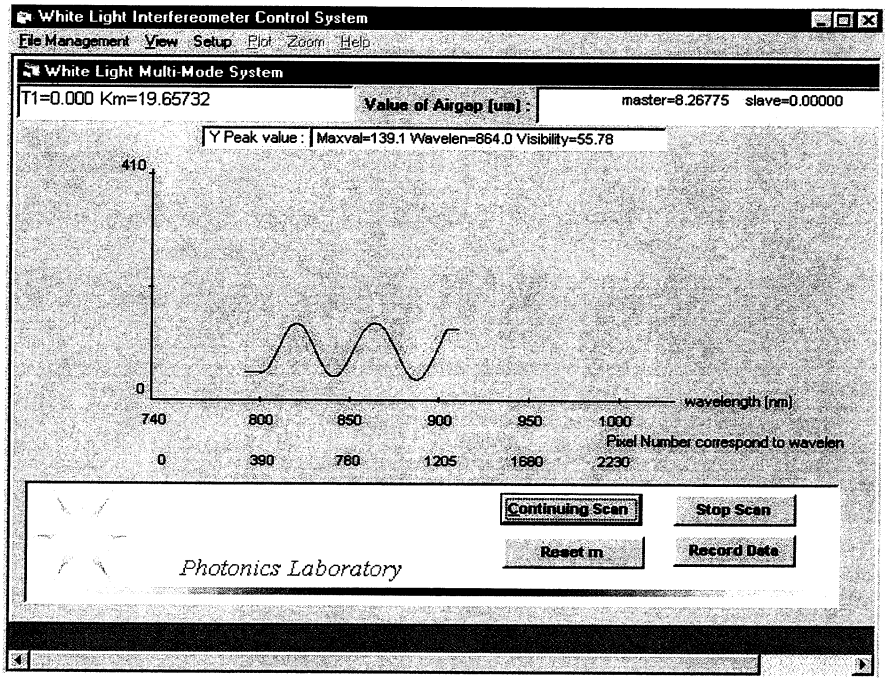

(b) Normalized interference spectrum

Figure 2.3. Illustration of the white interference spectrum signal processing

Thus the phase difference between these two spectral components is given by

$$\Delta\varphi = \varphi_1 - \varphi_2 = \frac{4\pi(\lambda_2 - \lambda_1)}{\lambda_1\lambda_2} \qquad \text{----------(6)}$$

Rewriting Equation **(6)**, we have

$$L = \frac{\Delta\varphi \cdot \lambda_1 \cdot \lambda_2}{4\pi(\lambda_2 - \lambda_1)} \qquad \text{----------(7)}$$

If the phase difference of these two spectral components is known, the absolute value of the sensor air gap length L can be calculated by Equation (7). For example, the phase difference between two adjacent peaks is 2π. Therefore, by detecting the spectral locations of the peaks in the interference spectrum, we can determine the sensor cavity length L with Equation **(7).**

2.3 Experimental Results

This section details the sensor fabrication and some preliminary experimental results.

In order to evaluate the feasibility of the whitelight interferometric fiber strain gage for strain measurement, a Fabry-Perot interferometer was constructed by aligning two silica fibers collinearly with micron gaps between two well cleaved fiber ends, as illustrated in Figure 2.4. After the two fibers were inserted in the capillary tubing and were positioned to optimize the optical alignment, the sensor head was attached to an alumina plate using Cotronics alumina cement. The stainless steel, copper and brass are also tested as substrates. Figure 2.5 is White-light Interferometer Control System. Figure 2.6 is Micromotion Position System, which is used for sensor precise alignment to form a fiber optic interferometer.

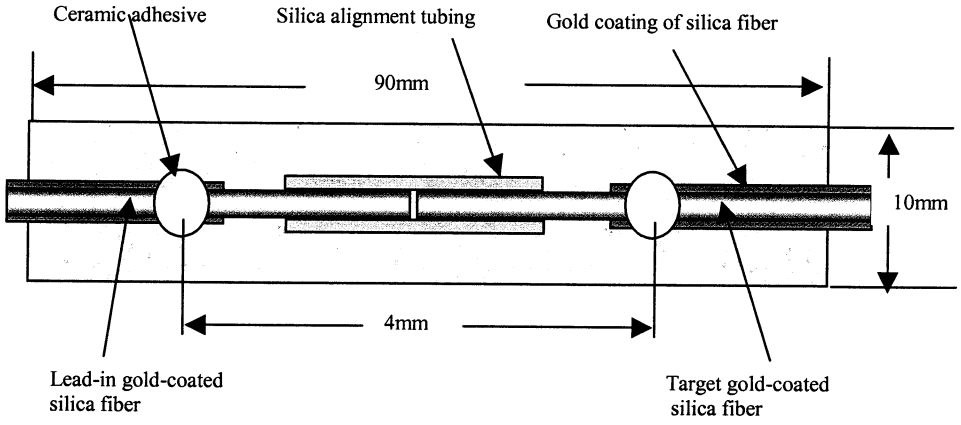

Figure 2.4. Details of construction of silica fiber interferometric strain gage.

Bonding the high temperature strain sensor on a substrate is a key issue for the strain sensor testing. Various sensor bonding methods will be discussed in detail later in this section.

For convenience room temperature test, a large alumina substrate was clamped at one end, and a micrometer was used to bend the substrate with a measured displacement at the other end, as depicted in Figure 2.7, 2.8

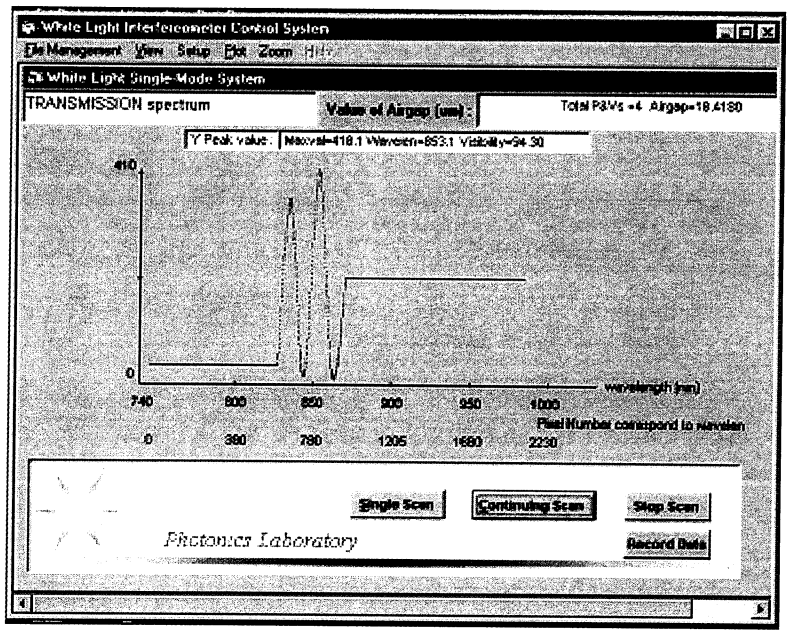

Figure 2.5. White-light Interferometer Control System used for monitoring the strain sensor fabrication and strain measurement.

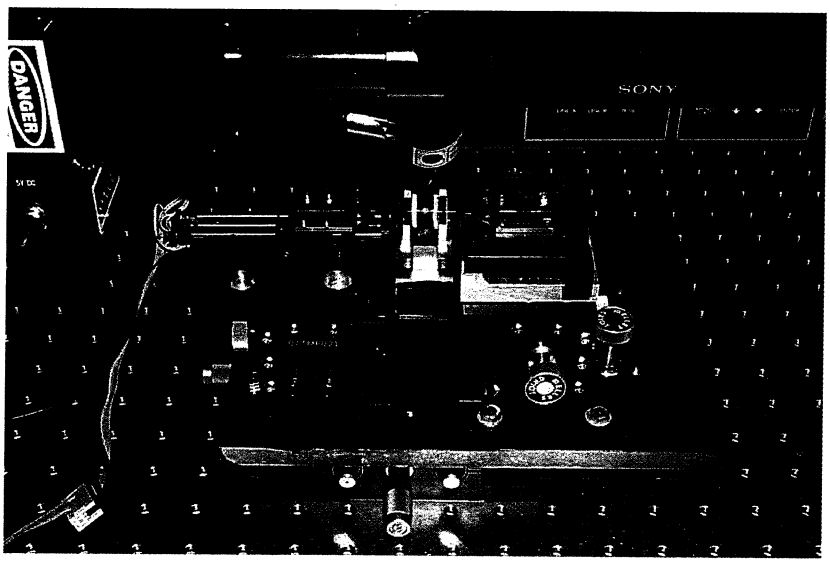

Figure 2.6. Micromotion Position System.

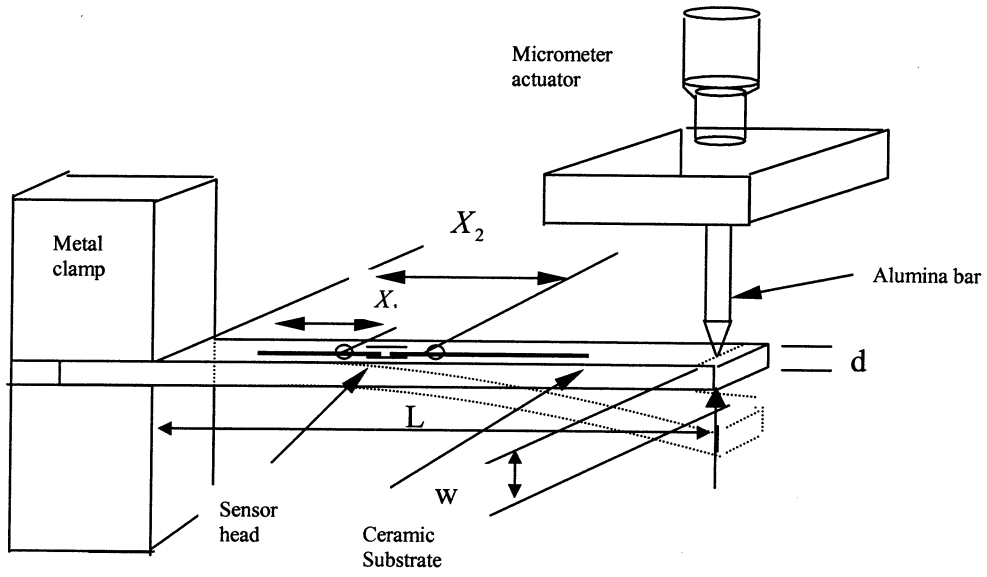

Figure 2.7. Experimental set-up of a fix-free cantilever beam used to develop strain in silica fiber strain gage.

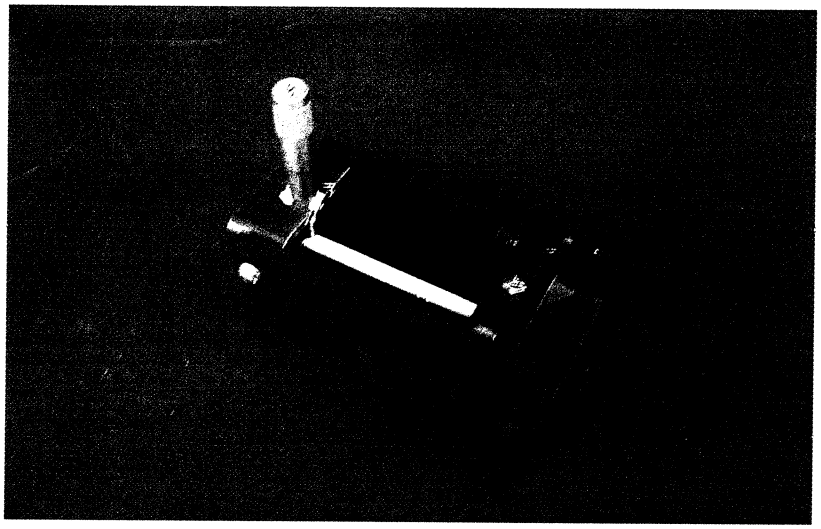

Figure 2.8. Actual experimental set-up of a fix-free cantilever beam.

From experimental mechanics, the displacement Δx of a point on the surface of a fixed-free cantilever beam can be related to the displacement W of the tip by

$$\Delta x = \frac{3wd}{2L^3}\left(LX - \frac{X^2}{2}\right)_{X_1}^{X_2} \qquad \text{----------(8)}$$

here, X_1 is the distance from the beam root to the first sensor bonding point, X_2 is the distance from the root to the second bonding point, w is the vertical deflection of the tip, L is the effective length of the beam (substrate), and d is the thickness of the beam.

Once the elongation Δx is known, the strain may be calculated as

$$\varepsilon = \frac{\Delta X}{X_2 - X_1} \qquad \text{----------(9)}$$

In one experiment, X_1 =25mm, X_2=29mm, L=91mm, and d=0.96mm.

The first step in the experiment was to confirm the operation of strain gage at room temperature. The tip of the substrate is displaced in 2μm increment, and the strain is calculated and measured by Equation (8) and by the white-light interferometric fiber strain sensor, respectively. Figure 2.8.1 shows the applied and the measured air gap tested at room temperature. As Figure 2.9 shows, the applied and the measured strain show an excellent agreement.

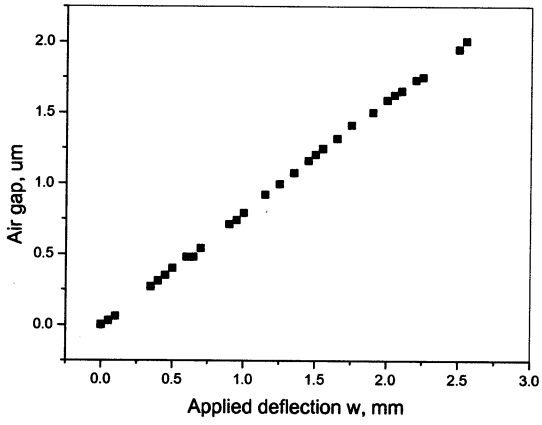

Figure 2.8.1. Applied and measured air gap tested at room temperature.

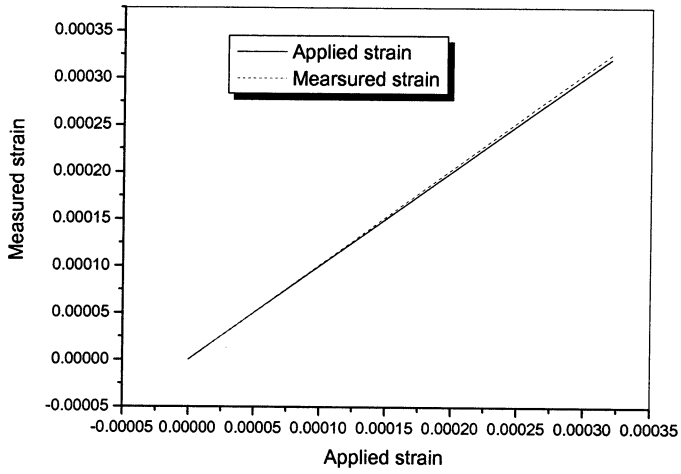

Figure 2.9. Applied and measured strains show good agreement.

To test the operation of the strain gage at high temperature, the alumina substrate with the silica fiber strain gage was inserted into an electronically controlled furnace. The photograph is shown in Figure 2.10.

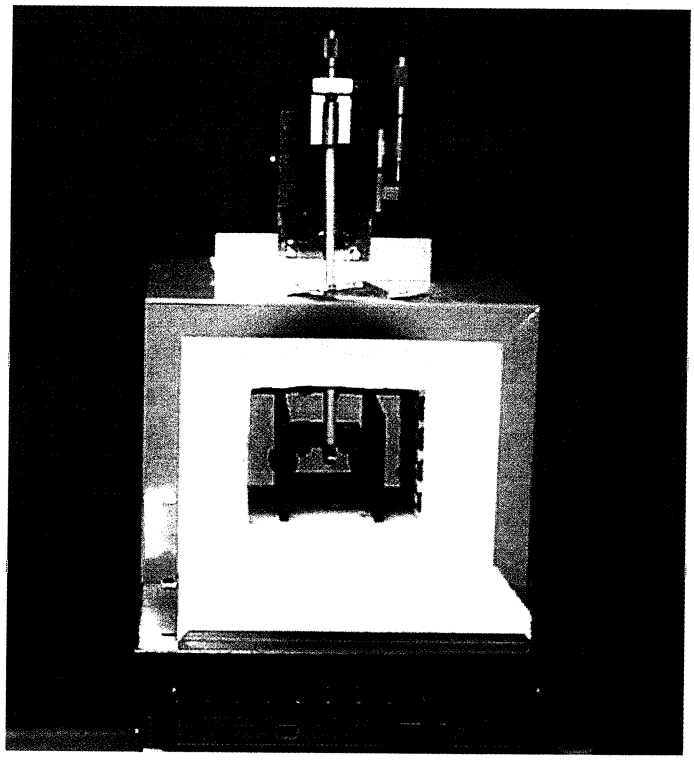

Figure 2.10. Experimental set-up used for the high temperature strain test.

The silica fiber strain gage is mounted on the substrate and is mounted on a specially designed steel holder, which can be positioned in the chamber of the furnace. On the top of the furnace is two micrometers with an alumina bar, which is used to displace the tip of the alumina.
The temperature was increased to 850°C at step of 100°C. At each step, the temperature is stabilized for at lease 15 minutes and the air gap is then recorded. Figure 2.10 is experimental set-up used for the high temperature strain test. Figure 2.10.1 is graphical illustration of the set-up. Result is shown in Figure 2.11.

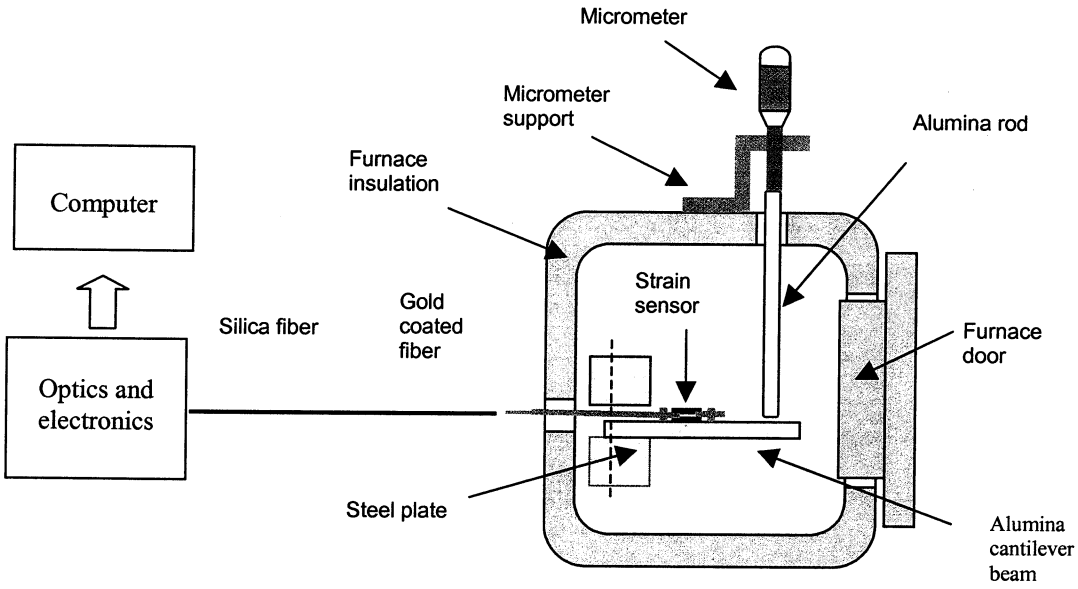

Figure 2.10.1. Graphical illustration of experimental set-up used to test the strain measurement with the white light system.

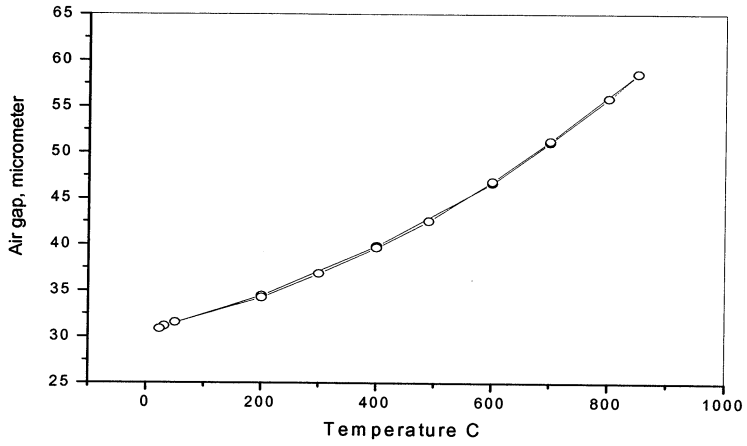

Figure 2.11. Air gap change induced by substrate strain and fiber thermal expansion at 850°C.

After the temperature was stabilized at 800°C and 850°C for 15 minutes each, the tip of the alumina substrate was displaced by adjusting the vertical micrometer on a micropositioner. The measured strain was compared to the calculated strain over a range from zero to 600 mirostrain. Figures 2.12 and 2.14 indicate linear relationship between the air gap and the applied deflection. Figures 2.13 and 2.15 indicate that the relationship is linear, and that the measured strain shows good agreement with the calculated strain.

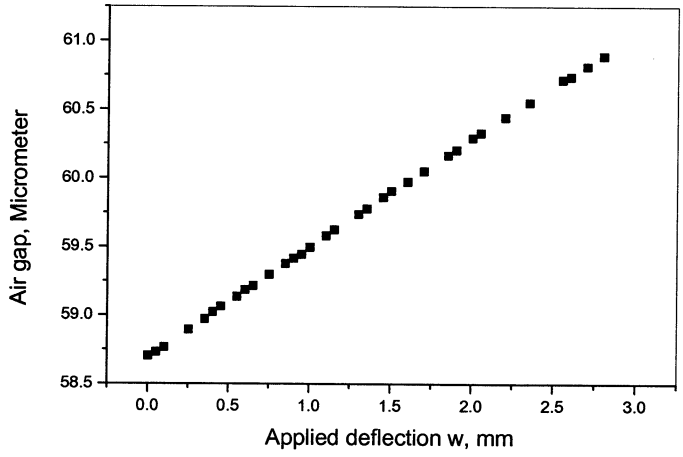

Figure 2.12. Applied deflection and the measured air gap at 850°C.

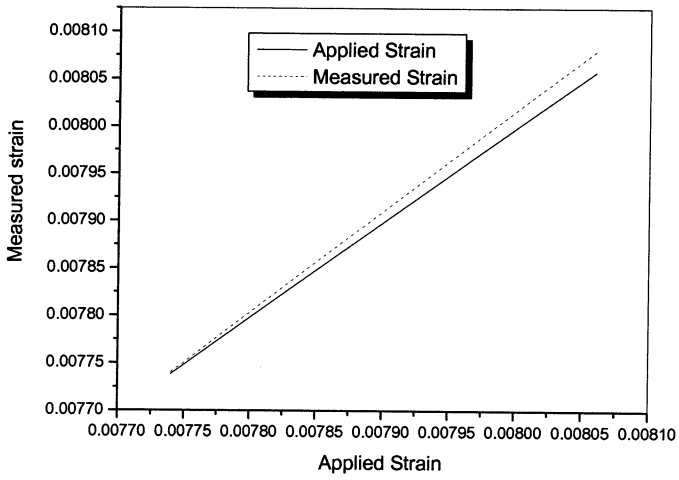

Figure 2.13. Agreement between measured strain. and calculated strain at 850°C.

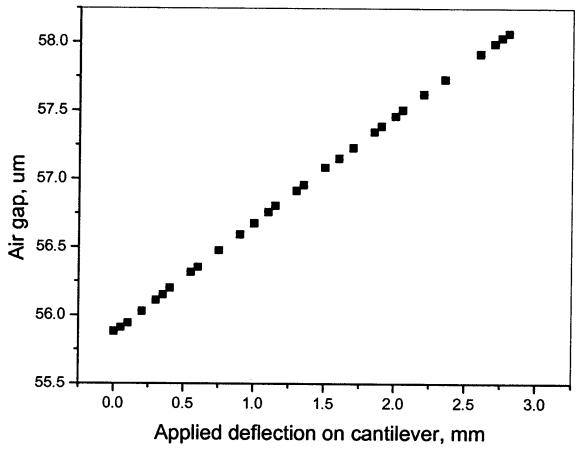

Figure 2.14. Applied deflection and the measured air gap at 800°C.

As shown in Figure 2.15, the air gap change has linear relation with the applied deflection at different temperatures.

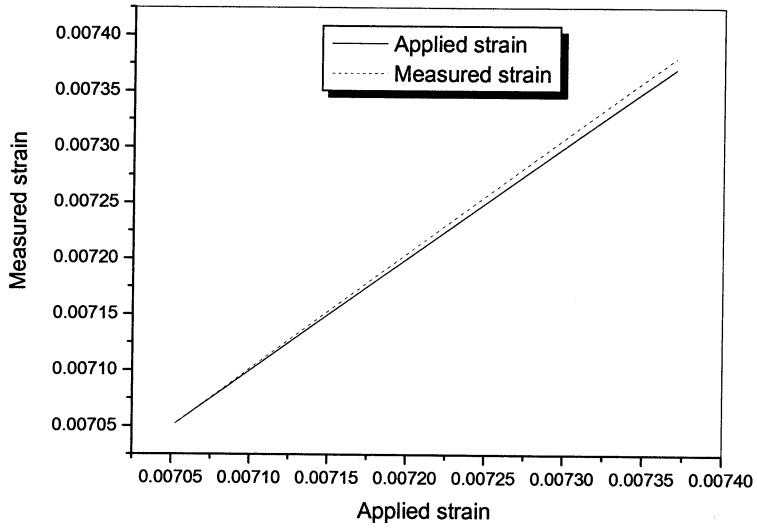

Figure 2.15. Agreement between measured strain and applied strain at 800°C

The temperature is stabilized at 800 °C and 850 °C, separately, for several days as shown in Figure 2.16. The value of the air gap remains almost the same at 800°C and 850°C within 400 hours. The fringe visibility is stable and is recorded as shown in Figure 2.17. These experiment results show that the gold-coated silica fiber-based strain sensor is durable and very stable over the test period.

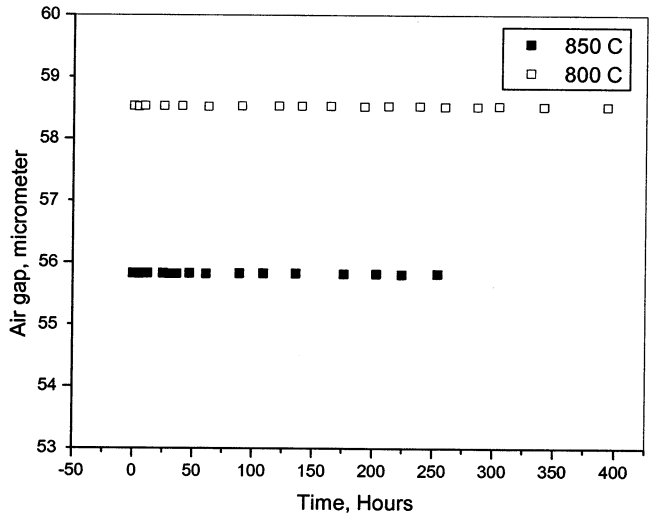

Figure 2.16. Air gap is stable at 800°C and 850°C.

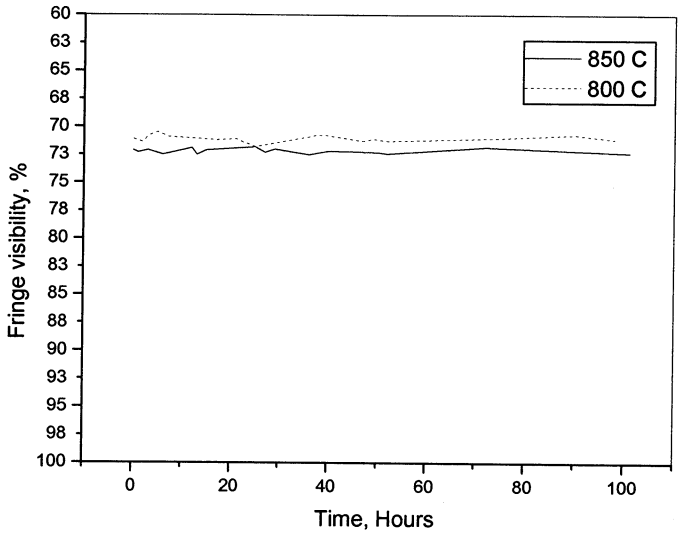

Figure 2.17. Fringe visibility at room temperature, 800°C, 850°C with time increment for 100 hours.

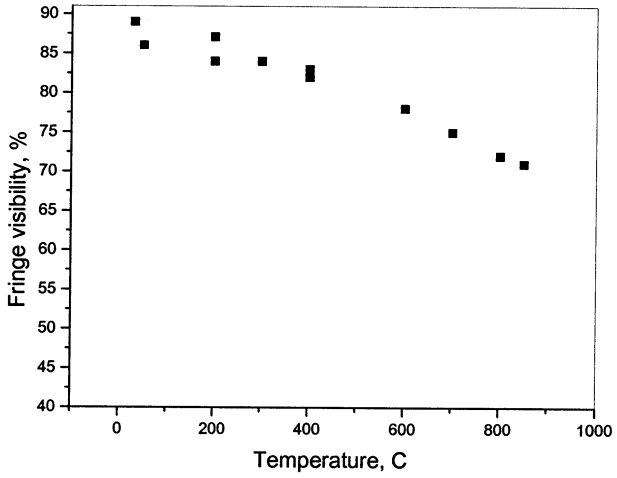

Figure 2.18. Fringe visibility decreases with temperature increment.

Figure 2.18 indicates the Fringe visibility decreases with the displacement caused by temperature rising. At room temperature, deflection is applied on the cantilever, the air gap is measured by the white light interferometer system, as indicated in Figure 2.19. The lowest line in the Figure 2.19 is the air gap at room temperature. Further analysis shows the measured air gap on the lowest line is not a smooth line.

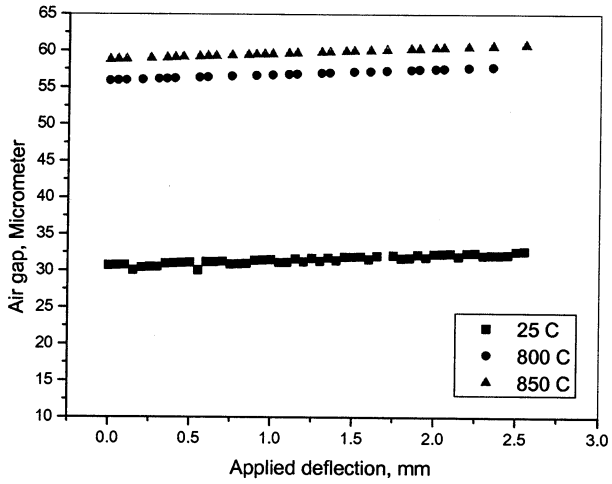

Figure 2.19. Linear relation between the applied deflection and measured air gap obtained at 23°C, 800°C and 850°C.

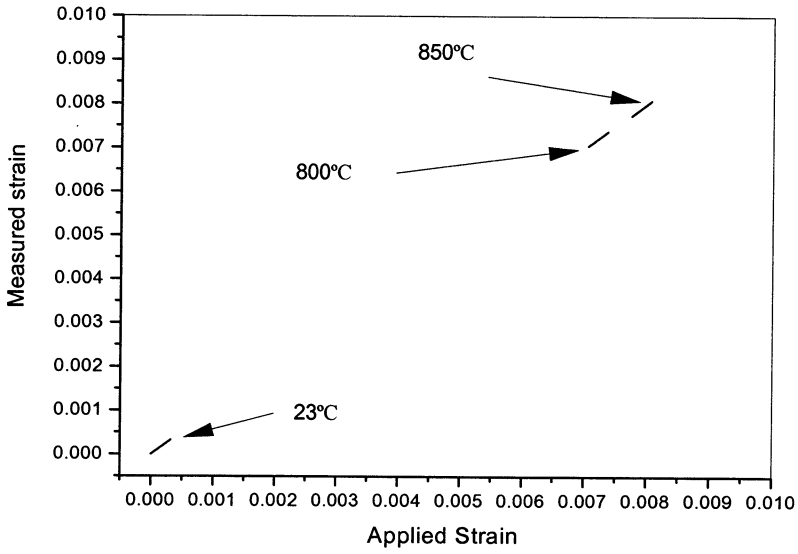

Figure 2.20. Linear relation between measured strain and applied strain at 23°C, 800°C and 850°C.

In the strain sensor experiment at room temperature, readout of the air gap of the single mode white light system with the increment of the applied deflection is shown in Figure 2.21.

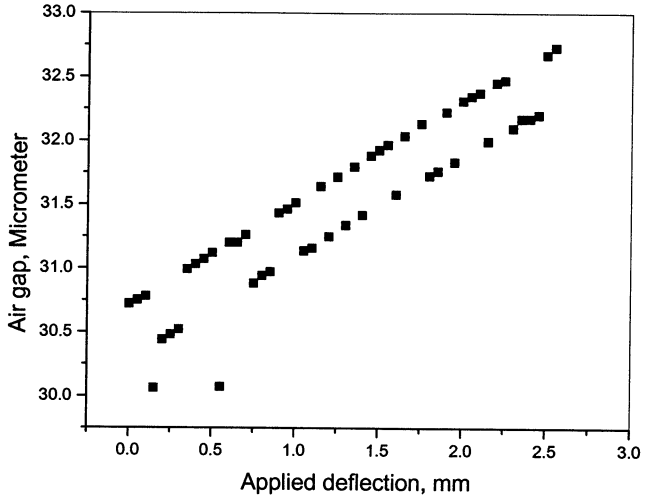

Figure 2.21. Air gap change with applied deflection at room temperature

The air gap has some jumping (about 400nm) with the applied deflection increment of 50μm step, about half of the 850nm wavelength of the LED in the single mode white light system. The readout data could be further improved by proper software modifications.

Steel and copper are also tested as substrates, as shown in Figures 2.22 and 2.23. The single-mode fiber strain sensor based on the white light system can measure air gaps up to 100μm in these experiments.

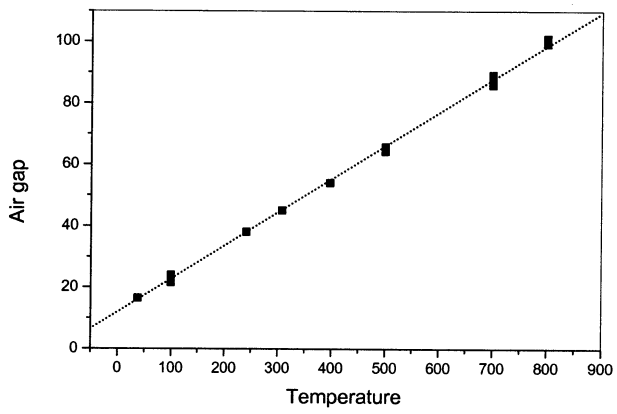

Figure 2.22. Air gap increases with temperature increases, the strain sensor is bonded on a copper substrate.

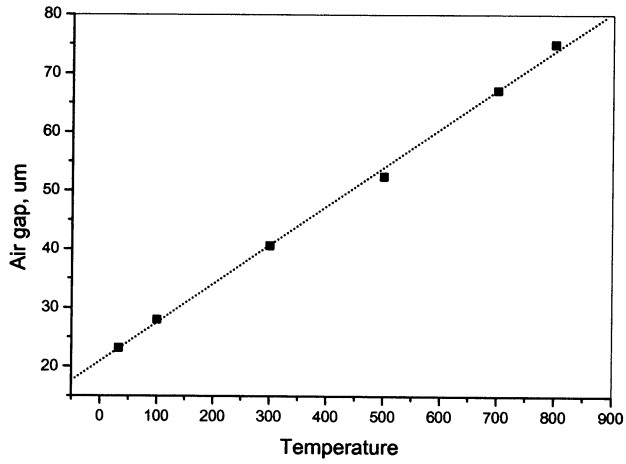

Figure 2.23. Air gap increases with temperature increment, the strain sensor is bonded on a steel substrate.

3 Conclusions

During the twelve months of the program, one complete sensor system was designed, developed and demonstrated for high temperature strain measurement. This system is based on fiber optic white-light interferometry.

An experiment set-up was constructed to permit testing of strain measurements at temperatures up to 850°C, Using this experimental setup, excellent results were obtained for strain measurement at temperatures up to 850°C by mounting the strain gage on an alumina beam or a metal beam in a furnace.